

## Changes in seismicity in a volcanically active region of the Izu Peninsula, Japan

K. Z. Nanjo,<sup>a,b,c,d,\*</sup>, Y. Yukutake<sup>e</sup>, T. Kumazawa<sup>c</sup>

<sup>a</sup>*Global Center for Asian and Regional Research, University of Shizuoka, 3-6-1 Takajo, Aoi-ku, Shizuoka 420-0839, Japan*

<sup>b</sup>*Center for Integrated Research and Education of Natural Hazards, Shizuoka University, 836 Oya, Suruga-ku, Shizuoka 422-8529, Japan*

<sup>c</sup>*Institute of Statistical Mathematics, 10-3 Midori-cho, Tachikawa, Tokyo 190-8562, Japan*

<sup>d</sup>*Japan Agency for Marine-Earth Science and Technology, Yokohama Institute for Earth Sciences, 3173-25 Showa-machi, Kanazawa-ku, Yokohama, Kanagawa 236-0001, Japan*

<sup>e</sup>*Earthquake Research Institute, The University of Tokyo, 1-1-1 Yayoi, Bunkyo-ku, Tokyo 113-0032, Japan*

\*Correspondence and requests for materials should be addressed to K.Z.N. (email: nanjo@u-shizuoka-ken.ac.jp)

ORCID: 0000-0003-2867-9185 (K. Z. N.); 0000-0002-1533-4885 (Y. Y.); 0000-0003-2435-640X (T. K.)

### Highlights

- Deep low-frequency earthquakes in Izu Peninsula, Japan, showed seismic quiescence
- Shallow ordinary earthquakes in the same region showed similar quiescence
- The start of quiescence for both types of earthquakes was almost coincidental
- Seismic quiescence occurred with no significant uplift during the study period
- Magma source, causing an uplift, implies a transition phase to an inactive state

## ABSTRACT

The eastern side of the Izu Peninsula in Japan is volcanically and seismically active. In this region, earthquake swarms of ordinary earthquakes frequently occur at shallow depths, and this is considered to be associated with magma intrusion. Beneath ordinary earthquakes, low-frequency earthquakes (LFEs) are infrequently observed. To better understand the characteristics of LFEs, we produced an LFE catalog for 2005-2020, using the matched-filter method. We then conducted a timeseries analysis based on the Epidemic-Type Aftershock Sequence model, showing relative quiescence (change in occurrence rate, which became quiet). For comparison, the same analysis was conducted by using the Japan Meteorological Agency catalog of ordinary earthquakes, showing a similar result. The change points for both types of earthquakes fell sometime between late 2009 and mid-2013, during which two out of three swarms of ordinary earthquakes occurred. We associated the quiescence with a decrease in background rate, where background rate, by removing the triggering effect of aftershocks, is known to be caused directly by the magma source, which can vary with time. We further discussed surface displacement data obtained from the Geospatial Information Authority of Japan, showing that the uplift due to magma intrusion was significant during the 1970s-1990s, although it was in abatement or unobservable during the study period (2005-2020). We interpreted the quiescence with no significant uplift as an indication that magma source, which caused magma intrusion into the study region, is in a transition phase, becoming less active, compared with the magma source during the 1970s-1990s.

## *Keywords:*

Volcano monitoring; Intra-plate processes; Seismicity and tectonics; Volcano seismology; Computational seismology; Asia

## 1. Introduction

The Izu Peninsula in central Japan is in the northern most part of the Izu Bonin Mariana (IBM) Arc and is located in the collision zone with Honshu Island, where crustal deformation is active (Fig. 1). This Peninsula is volcanically and seismically active (Aramaki and Hamuno, 1977). The eastern side of the Izu Peninsula is a monogenic volcano field whose volcanoes are included in the Izu-Tobu Volcano Group (Koyama and Umino, 1991). This Volcano Group is listed as an active volcano where the Japan Meteorological Agency (JMA) operates 24-hours monitoring in a real-time manner. In the 1920s-1930s and 1970s-1990s, earthquake swarms, which consist of seismicity that lacks an obvious mainshock-aftershock sequence, and crustal deformation actively occurred, and these were associated with magmatic activities (Geospatial Information Authority of Japan, 2016; Shishikura et al., 2023). Hereafter, the Geospatial Information Authority of Japan is referred to as GSI. Ishida (1984) investigated the spatial temporal variation of an earthquake swarm that migrated to trigger the 1980 Izu-Hanto-Toho-Oki earthquake of magnitude ( $M$ ) 6.7. Shimazaki (1988) suggested a dyke intrusion mechanism as a possible source of persistent swarms in the region east of the Izu Peninsula. Furthermore, associated with swarm activity in 1988, Tada and Hashimoto (1989) proposed a model of tensile fault to account for the horizontal and vertical displacement fields around the eastern part of Izu Peninsula.

In 1989, an eruption occurred off the east coast of Izu Peninsula after the start of earthquake swarms, then formed the Teishi Knoll (e.g., Yamamoto et al., 1991; Nagamune et al., 1992), which is one of the members of the Izu-Tobu Volcano Group. Geodetic and seismic data have been analyzed to explain these swarms on the basis of the dike intrusion process (Okada and Yamamoto, 1991; Okada et al., 2000; Hayashi and Morita, 2003; Morita et al., 2006; Miyamura et al., 2010). Okada and Yamamoto (1991) proposed a model, based on seismic and geodetic data, that consisted of two tensile faults corresponding to a series of magma intrusions, and a right-lateral reverse fault representing a  $M5.5$  earthquake, corresponding to the largest event in this swarm. Using their model, Okada and Yamamoto (1991) discussed their data in relation to magmatic activity.

The swarm activity in 1998 was also accompanied by crustal deformation, and was well modelled by the dyke opening process (Okada et al., 2000). The swarm's hypocenters in 1998, which were precisely defined, were mainly aligned on a thin vertical plane (Hayashi and Morita, 2003; Morita et al., 2006). The normal direction to the plane coincided well with the direction of tectonic extensional stress around the hypocentral area (Ukawa, 1991). At the beginning of activity, a small fraction of the events occurred at a greater depth, where hypocenters aligned on a vertical line and migrated upward. After one day from the beginning, hypocenters reflected an expansion downward and

upward of the dyke from the center of the swarm by excess magma pressure on the inside (Hayashi and Morita, 2003; Morita et al., 2006).

Miyamura et al. (2010) found that the duration of earthquake swarms in the Izu region was associated with the largest variation in the volumetric strain records at the Higashi-Izu JMA station within 24 hours from the early stages of the swarms. Consequently, in 2010, the Japan governmental Earthquake Research Committee (ERC) investigated the statistical relationships between the volumetric strain records and seismicity to forecast the magnitudes of swarm activities (ERC, 2010). Kumazawa et al. (2016) used the Epidemic-Type Aftershock Sequence (ETAS) model (Ogata, 1988) on eight swarms after mid-1980 to explore their relationship with the volumetric strain recorded by the Higashi-Izu JMA station (Fig. 1). They proposed that the ETAS model may be helpful in monitoring magma intrusions that drive changes in stress.

While swarms occur at a depth range of  $<20$  km (black symbols in Fig. 1), earthquakes during non-swarm periods also occur at the same depth range. These are high-frequency and ordinary earthquakes while low-frequency earthquakes (LFEs) occur at a depth range of 30–40 km (red symbols in Fig. 1). Using the earthquake catalog maintained by JMA, more than 10,000 ordinary earthquakes occurred during 2005–2020, and there were swarms in 2006, 2009, and 2011 (Fig. 2). On the other hand, LFEs were observed 47 times during the same period. JMA, which employs conventional event-detection methods, has difficulty in detecting LFEs that are easily buried in noise due to their low signal-to-noise ratios. If a LFE catalog is produced by using the matched-filter (MF) method, which cross-correlates a template to continuous seismic signals (Yukutake, 2017; Yukutake et al., 2019), it could resolve this difficulty, and be used to find characteristics of LFEs.

The primary purpose of this study is to clarify the characteristics of time-dependent activity of LFEs, using the ETAS model. For the ETAS analysis, we produced a LFE catalog using the MF method. Our resultant catalog included 895 LFEs during the 2005–2020 period. This is about 19 times more than the number of earthquakes (47) reported by JMA during the same period. This means that LFEs occurred more frequently than were previously thought. For comparison, the same model as the time-dependent activity of LFEs was used for that of ordinary earthquakes.

Our study region, indicated by a black rectangle in Figs. 1b and 2b, is referred to in this paper as the Izu-Tobu region. This region was defined to include the main activity of three earthquake swarms in 2006, 2009, and 2011, and most LFEs that are located almost immediately below ordinary earthquakes in 2005–2020 of the JMA catalog (Fig. 1).

## 2. Data

### *2.1. LFEs and ordinary earthquakes in the JMA catalog*

The JMA catalog includes ordinary earthquakes and LFEs in Japan. Although ordinary earthquakes are distributed all over Japan, LFEs tend to concentrate beneath active volcanoes, along the boundary between the Philippine Sea Plate and the continental plate in western Japan (Obara, 2002), and as several isolated clusters in the intraplate regions (Aso et al., 2013). Each event in the JMA catalog is classified based on subsidiary information, such as natural (ordinary) earthquakes, LFEs, artificial events, and others.

An assessment of the ordinary earthquakes in the Izu-Tobu region during 2005-2020 showed that the three seismic swarms started in 2006, 2009, and 2011 (Fig. 2) and their respective periods of main activities were Mar. 1-Apr. 30, 2006, Dec. 17-21, 2009, and Jul. 17-18, 2011 (GSI, 2016). The locations of these swarms overlapped or were close to each other. Their depths ranged from 0 to 20 km (Fig. 1c). This is consistent with a previous swarm that started in 1989 (Hayashi and Morita, 2003; Morita et al., 2006). LFEs in the Izu-Tobu region were separated from those in other regions (Fig. 1a). LFEs occurred at depth of 30-40 km beneath ordinary earthquakes (Fig. 1).

The number of ordinary earthquakes with  $M \geq -1$  within the study region in 2005-2020 is more than 10,000, while the number of LFEs with  $M \geq -1$  is 47. We used these ordinary earthquakes in the JMA catalog for further analysis (see Data availability). On the other hand, given that the number of LFEs is small, we thought that the characteristics of LFEs are not fully understood. Given that LFEs in the Izu-Tobu region are deeper than ordinary earthquakes, and due to the low signal-to-noise ratios of LFEs, it is likely difficult to detect LFEs with conventional event-detection methods employed by JMA.

### *2.2. The MF method for LFEs*

We produced a catalog of LFEs using the MF method (Shelly et al., 2007; Peng and Zhao, 2009; Kato et al., 2012; Yukutake, 2017; Ross et al., 2019). In this study, the MF system used for detecting LFEs beneath the Hakone volcano in Japan (Yukutake, 2017; Yukutake et al., 2019) was modified so that it was applicable to the Izu-Tobu region. Waveforms of continuous signals that were used in this study covered the Jan. 2005-Dec. 2020 period, as recorded by 20 seismic stations (Fig. 3a) with a three-component velocity seismometer in and around the Izu-Tobu region (see Data availability).

To prepare template LFEs, we used the JMA catalog to select events classified as LFEs in the Izu-Tobu region (see Data availability). This study relied on statistical analyses of the LFE catalog, which covered the studied time interval. It should be noted that the catalog may be controlled by the selection of template earthquakes in the MF analysis. Large LFEs with  $M \geq 0.2$  were selected in order

to allow template waveforms to include more information on signals than on noise. Then, among them, LFEs that were recorded by six stations with a minimum signal-to-noise-ratio of 2 were selected (Yukutake et al., 2019).

The MF procedure to identify LFEs, briefly described in this paragraph, is the same as that of Yukutake (2017) and Yukutake et al. (2019). Three-component waveform records for each template LFE were used, applying a six-second time window beginning two seconds before the onset time of the theoretical S-wave arrivals. Both templates and continuous waveforms were bandpass-filtered for 1-6 Hz and decimated at 20 Hz to reduce the calculation cost. This band was selected according to Yukutake (2017) and Yukutake et al. (2019), although other studies used a slightly narrower band, such as 1-4 Hz by Kurihara and Obara (2021). The correlation coefficients (*CC*) between a template and continuous waveform at each sampling time for every component at each station were calculated. After subtracting the hypocenter-to-station travel time of the theoretical S-wave, the time sequences of the correlation function throughout all channels were stacked. When the peak of the stacked correlation function exceeded a threshold level of nine times the median absolute deviation, an event was identified as a candidate LFE. After removing multiple counts, the location of the candidate was assigned to the hypocenter of the matched template LFE determined by JMA. Magnitude was determined as the mean of the maximum amplitude ratios of the template with respect to the candidate. The MF procedure described above was applied to all waveform records in the period Jan. 2005-Dec. 2020, and a preliminary catalog, including candidate LFEs, was created, although LFEs identified by five or less stations were not included in this catalog.

### 2.3. LFE catalog

Less reliable LFEs were removed from the preliminary catalog to create a finalized catalog, as follows. Among candidate LFEs, false detection occasionally occurred due to contamination by other seismic signals such as teleseismic earthquakes. This contamination led to the detection of LFEs with a large *M*, so we visually inspected whether each template LFE was used to detect many candidate LFEs with  $M > 1.5$ , a magnitude above which LFEs have never been recorded by JMA in the Izu-Tobu region since 2005. We considered that such template LFEs had a feature similar to teleseismic earthquakes and decided to eliminate them from the list of template LFEs. Thus, candidate LFEs detected by using the eliminated template LFEs were removed from the preliminary catalog, resulting in the intermediate catalog that included 2502 LFEs. Despite this quality test, an additional test was conducted, as described in the following paragraphs.

The *CC*-values of LFEs in the intermediate catalog (Fig. 3b) ranged between 0.1 (poor correlation

with a template LFE) and 1 (strong correlation with, and identical to, the corresponding template LFE). Setting the minimum  $CC$  to a low value implies the use of an incomplete catalog influenced by the nature of low signal-to-noise ratios of LFEs. The minimum threshold for  $CC$  ( $CC_{th}$ ), above which LFEs are included in the finalized catalog and used for our analysis, should be above the upper noise limit. Histograms of  $CC$ -values in Fig. 3b show an asymmetric distribution with a tall peak at  $CC \sim 0.15$ . We followed previous studies (Green and Neuberg, 2006; Petersen, 2007; Lamb et al., 2015), in which the distribution of lower  $CC$ -values was modeled by a normally distributed curve that would be expected for random correlations between signals and noise, while the upper tail was considered to represent the presence of well-correlated LFEs. Visual inspection shows that frequencies at and below  $CC \sim 0.15$  are in good agreement with the left-hand side of the normally distributed curve where the mean is 0.155 and its standard deviation is 0.02 (Fig. 3b). We selected  $CC_{th}=0.25$ , which is larger than the mean plus three standard deviations. The histogram for  $M \geq 0$  is also displayed because our analysis basically did not include LFEs with  $M < 0$ . A total of 35 template LFEs were used for the intermediate catalog.

The number of LFEs (894) in our finalized catalog of  $CC_{th}=0.25$  (Fig. 3c) is about 19 times larger than in the JMA catalog, which lists 47 LFEs detected in 2005-2020 by a conventional method that is not based on  $CC$ .

The scope of this study did not permit us to reveal repeating LFEs, nor cyclic activities and cluster characteristics, as were studied by Lamb et al. (2015). Rather, this scope was to resolve the difficulty in detecting smaller LFEs. Our future research will conduct in-depth analyses of repeating LFEs for each cluster in the Izu-Tobu region, referring to Lamb et al. (2015), and using a sophisticated MF method that can locate detected LFEs to appreciate whether they occurred in the same cluster as the template LFE used to find them.

### 3. Methods

#### 3.1. Change point analysis

The ETAS model (Ogata, 1988) was originally introduced for ordinary earthquakes, but this model was also used for LFEs in the present study. We conducted a change point analysis using the ETAS model and the Akaike Information Criterion (AIC) (Akaike, 1974). Details of this analysis were provided by Kumazawa et al. (2019). Unlike Kumazawa et al. (2019), to conduct this analysis,  $\Delta AIC = AIC_{single} - AIC_{2stage}$  was used as a function of the change-point time  $T_c$ . Here,  $AIC_{single}$  is AIC for the standard (single) ETAS model that considers constant parameter values over time, and  $AIC_{2stage}$  is AIC for the two-stage ETAS model that considers different parameter values in

subperiods before and after  $T_c$ , where both models are fitted to LFEs of  $M \geq M_{th}$  (threshold magnitude). If  $\Delta AIC \geq 2q$ , the two-stage model is better fitted to the data than the single model, detecting candidate changes in occurrence rate, where  $q$  is the degree of freedom to search for the best candidate  $T_c$  from the data.  $q$  depends on sample size (number of LFEs) (Ogata, 1992; Kumazawa et al., 2010), and increases with sample size. Given that  $\Delta AIC \geq 2q$  was observed, a change point's confidence interval of 68% was calculated (e.g., Kumazawa et al., 2010). The same analysis was conducted for the time-dependent activity of ordinary earthquakes.

### 3.2. Choice of $M_{th}$

Analyses of the ETAS model of LFEs during a specified time interval are critically dependent on the choice of the  $M_{th}$  value. To select it, we referred to estimates of completeness magnitude ( $M_c$ ) of the processed data of LFEs. Above  $M_c$ , all LFEs are considered to be detected. If  $M_{th}$  is too low, compared to estimates of  $M_c$ , then it leads to an unreliable ETAS fitting.

To compute  $M_c$ , we employed the Entire-Magnitude-Range (EMR) technique (Woessner and Wiemer, 2005), based on the Gutenberg-Richter (GR) relation (Gutenberg and Richter, 1944), given by  $\log_{10}N = a - bM$ , where  $N$  is the number of LFEs with a magnitude larger than or equal to  $M$  in the given time window, and  $a$  and  $b$  are constants (e.g., Nanjo and Yoshida, 2018; Nanjo, 2020; Nanjo et al., 2023). Statistical modeling was performed to distinguish between completely detected and incompletely detected parts of the frequency-magnitude distribution (Woessner and Wiemer, 2005).  $M_c$  is the magnitude at which these parts are separated. The  $b$ - and  $a$ -values were computed based on earthquakes in the completely detected part above  $M_c$ . We also computed uncertainty in  $M_c$  based on a bootstrapping technique (Schorlemmer et al., 2003).

$M_c$  for LFEs was about 0.2~0.4, based on catalogs covering three periods: 2005-2009, 2010-2014, and 2015-2020 (Fig. 4). We chose  $M_{th}=0.3$  ( $M \geq 0.3$ ) for analyses of the ETAS model of LFEs. We also considered  $M_{th}=0.4$  ( $M \geq 0.4$ ) to suggest a generally stable feature.

Similar to the LFEs, we estimated  $M_c$  values for ordinary earthquakes. A single value of  $M_c$  over the entire catalog was not considered, but timeseries of  $M_c$ , obtained from a moving window approach, was considered, where the window covered 100 ordinary earthquakes. The reason for adopting this moving window approach was to calculate the local properties of an input data stream and an output  $M_c$  variation.  $M_c$  values were generally about 1, except for the timing of the swarms in 2006 and 2009 where  $M_c$  values were above 1 (Fig. 4). We chose  $M_{th}=1$  ( $M \geq 1$ ) for analyses of the ETAS model of ordinary earthquakes. We also considered another value ( $M_{th}=1.5$ ) for the same reason as that described for LFEs.



## 4. Results

### 4.1. First-order timeseries analysis

We conducted a first-order timeseries analysis, based on the entire period from Jan. 2005 to Dec. 2020 (Fig. 5).  $\Delta\text{AIC}$  of LFEs as a function of  $T_c$  (Fig. 5b) shows that a change point's confidence interval (horizontal solid bars) was likely during the periods from mid-2012 to mid-2013 for  $M \geq 0.3$  (blue data) and from late 2011 to mid-2013 for  $M \geq 0.4$  (red data). The same analysis was conducted for ordinary earthquakes (Fig. 5a). The two-stage ETAS model was much better than the single ETAS model during  $T_c=480\text{--}4050$  days for  $M \geq 1$  (blue data). In this range of  $T_c$ , we observed three pronounced peaks in  $\Delta\text{AIC}$  at the timing of the three swarms (vertical orange, blue, and pink lines). The change point's confidence intervals (horizontal solid bars in blue) were likely from late 2009 to mid-2011, during which the 2009 and 2011 swarms occurred (vertical blue and pink lines). A similar feature was observed for  $M \geq 1.5$  (red data in Fig. 5a). It is generally seen that quiescence for the two types of earthquakes started around the timing of the 2009 and 2011 swarms. A detailed observation shows that the most significant  $T_c$ -values for ordinary earthquakes were earlier than those for LFEs.

LFEs ( $M \geq 0.3$ ) before  $T_c=2740$  days, indicated by a green circle in Fig. 5b, were fitted by the ETAS model (Fig. 6b). The occurrence rate (black) after  $T_c=2740$  days was smaller than the extrapolated rate (red), indicating the relative quiescence of LFE activity. Here, the extrapolated rate is the occurrence rate computed by using the ETAS model whose parameters were obtained by fitting to LFEs ( $M \geq 0.3$ ) before  $T_c=2740$  days. Ordinary earthquakes ( $M \geq 1$ ) until  $T_c=1820$  days (green circle in Fig. 5a) fitted by the ETAS model (Fig. 6a) show that the occurrence rate (black) after  $T_c=1820$  days was smaller than the extrapolated rate (red), indicating similar quiescence to LFEs (Fig. 6a).

The above result was not induced by inclusion of a period around the timing of the first swarm in 2006 into the study period (Jan. 2005-Dec. 2020). Namely, we examined whether quiescence starting around the timing of the second and third swarms in 2009 and 2011 appeared to remain stable without a period around the timing of the first swarm in 2006 (Fig. 7). To examine this, we conducted a timeseries analysis of ordinary earthquakes and LFEs during the subperiod Jan. 2008-Dec. 2020. Results show that the general  $\Delta\text{AIC}$ - $T_c$  patterns (Fig. 7) for both types of earthquakes were similar to those during the corresponding period in Fig. 5. The change point's confidence interval coincided with the timing of the 2009 swarm for ordinary earthquakes, but it emerged during the period from mid-2012 to mid-2013 for LFEs.

#### 4.2. Second-order timeseries analysis

We conducted a second-order timeseries analysis, based on the subperiods Jan. 2005-Dec. 2010 for LFEs (Fig. 8b) and Jan. 2005-Dec. 2008 for ordinary earthquakes (Fig. 8a). We considered these subperiods because they were before the change point's confidence intervals seen in the results for the entire period (Fig. 5). The results of ordinary earthquakes and LFEs in Fig. 8 show that the change points' confidence intervals were limited to the timing of the 2006 swarm (vertical yellow bar). Detailed observation shows that the confidence intervals were later for LFEs than for ordinary earthquakes.  $\Delta AIC$  for LFEs with  $M_{th}=0.4$  (red data in Fig. 8b) shows a better but insignificant outcome when the two-stage ETAS model, rather than the single ETAS model, was used. Namely,  $\Delta AIC$  was higher than 0 ( $\Delta AIC > 0$ ), but it was below the horizontal dashed line, which is a hurdle to the selection of the two-stage ETAS model. We interpreted this insignificant outcome as an indication that the number of LFEs with  $M \geq 0.4$  was not enough to achieve the desired conclusion. Visual inspection of  $T_c$  (green circles in Fig. 8) shows quiescence of both types of earthquakes (Fig. 9).

Overall, the first-order observation was that quiescence for both types of earthquakes started during the period from late 2009 to mid-2013 when the 2009 and 2011 swarms occurred. Detailed observation showed that the start of quiescence was earlier for ordinary earthquakes than for LFEs. Beyond that, we showed that the second-order quiescence occurred before the start of the first-order quiescence. This second-order quiescence started around the timing of the 2006 swarm. Similar to the first-order timeseries analysis, detailed observation showed the earlier start of quiescence for ordinary earthquakes than for LFEs.

#### 4.3. Background rate

In the framework of the ETAS model, all earthquakes are decomposed into Poisson background activity and aftershock activity. Measuring the occurrence rate of the former activity ( $\mu$ ), separated by that of the latter activity, allows the magma source to be inferred (Kumazawa et al., 2016). The background rate means the rate of earthquake occurrence caused by either tectonic or magma sources that can vary with time (Kumazawa et al., 2016). Past studies (Hainzl and Ogata, 2005, Llenos et al., 2009, Llenos and McGuire, 2011, Brodsky and Lajoie, 2013) indicated that variation in stress affects the background rate.

Although a sophisticated nonstationary model is available (e.g., Kumazawa et al., 2016, 2019), this study adopted a simple approach to capture essential aspects of the time-dependent  $\mu$ . This involves taking a time-window approach. We considered the results obtained from the first-order

timeseries analysis (Jan. 2005-Dec. 2020), and compared  $\mu$  between the periods before and after  $T_c=2740$  days (green circle in Fig. 5). The results of LFEs (Fig. 6b) showed a larger  $\mu$ -value for the period before  $T_c=2740$  days ( $\mu=0.046$ ) (Fig. 6b) than for the period after it ( $\mu=0.022$ ). Similarly, the results of ordinary earthquakes (Fig. 6a) showed that  $\mu=0.019$  before  $T_c=1820$  days was larger than  $\mu=0.003$  after it. The same comparison in  $\mu$  was conducted for the second-order timeseries analysis of LFEs (Jan. 2005-Dec. 2010) and ordinary earthquakes (Jan. 2005-Dec. 2008). The result of  $\mu=0.069$  before  $T_c=620$  days (green circle in Fig. 8b) and  $\mu=0.029$  after it for LFEs (Fig. 9b) and  $\mu=0.024$  before  $T_c=480$  days (green circle in Fig. 8a) and  $\mu=0.010$  after it for ordinary earthquakes (Fig. 9a) showed a similar feature to that for the first-order timeseries analysis.

Earthquake swarms have been attributed to stress perturbations by magma intrusions (Einarsson and Brandsdottir, 1980; Dieterich et al., 2000; Okada et al., 2000; Toda et al., 2002; Waite and Smith, 2002; Feuillet et al., 2004; Smith et al., 2004) or fluid injections (Hainzl and Ogata, 2005; Lei et al., 2008; Terakawa et al., 2013; Terakawa, 2014). On the other hand, they can also be triggered by creep or slow-slip events (Ozawa et al., 2003; Delahaye et al., 2009; Segall et al., 2006). Thus, a swarm is thought to be driven by aseismic events that temporarily modify the stress state within the crust.

Kumazawa et al. (2016) studied eight swarms of ordinary earthquakes after mid-1980 to associate  $\mu$  with volumetric strain recorded by the strainmeter located at the Higashi-Izu JMA station (Fig. 1b). Given that the pattern of strain variation at this station depends on magma intrusion (ERC, 2010), they proposed that the ETAS model may help in monitoring magma intrusions that drive the changes in stress.

We associated the seismic quiescence observed in the first- and second-order timeseries analysis with a decrease in  $\mu$ . Similar to previous studies (Hainzl and Ogata, 2005; Llenos et al., 2009; Llenos and McGuire, 2011; Brodsky and Lajoie, 2013; Kumazawa et al., 2016), the decreases in  $\mu$  are attributed to variation in stress caused by the magma source.

## 5. Discussion

To compare the characteristics of the two types of earthquakes in the study region, we discuss crustal movement data. A leveling survey along the eastern coast of the Izu Peninsula since 1904 until 2015 (Fig. 10) showed secular variation of the four benchmarks (9335, 9336, 9337, 9338), where the reference benchmark is 9328 (GSI, 2016). The former four benchmarks were located in the Izu-Tobu region while the latter reference benchmark was located outside of the northern periphery of this region. The upward and downward crustal movement of the four benchmarks, relative to the reference benchmark, is interpreted as an indication of uplift and subsidence of the

Izu-Tobu region, respectively. A brief summary of crustal movement in the Izu-Tobu region is given as follows. The uplift progressed during the 1920s-1930s, where the 1923 *M*7.9 Kanto earthquake and the 1930 *M*7.3 Kita Izu earthquake occurred outside the Izu-Tobu region, while the 1930 swarm occurred inside the region. Until the early 1970s, pronounced crustal movement was not observed. Around the timing of the 1974 Izu Hanto-Oki earthquake, the uplift started to make noticeable progress. It continued until the late 1990s, after which the uplift was in abatement. After the 2009 swarm ended, an uplift was not observed.

Graphs of relative height of the four stations, numbered 1, 2, 3, and 4 in the reference station ODAWARA (Fig. 11a) and the reference station HATSUSHIMA (Fig. 11b), show no uplift, even after 2015, which is the last year of the leveling survey shown in Fig. 10. We selected the four stations and the two reference stations to consider the baselines, because we tried to mimic the configuration of the benchmarks used for the leveling survey (inset of Fig. 10). To create Fig. 11, we used station coordinates derived from the GNSS Earth Observation Network System (GEONET) (Muramatsu et al., 2021; Takamatsu et al., 2023). The product in the current GEONET analysis strategy is called the F5 solution while that in the previous strategy is called the F3 solution. Blue and red data in Fig. 11 were based on the F5 and F3 solutions, respectively. The F5 solution was used for the period Oct. 2013-Dec. 2020, because data in the most recent 10-year period were obtained. To complement data since Jan. 2005 (start of our study period), the F3 solution was used for the period Jan. 2005-May 2016. The F3 and F5 solutions overlapped during the period Oct. 2013-May 2016, providing justification for the consistency between these solutions (Fig. 11). Similarly, Fig. 12 was created for the reference station YUGAWARA-A, which was in operation since the end of Mar. 2017.

For all the baselines, fluctuations in relative height were observed, and some of them were associated with antenna replacement of stations (triangle) and tree trimming around stations (arrow). We also observed an increase in the order of a few centimeters in relative height around the timing of the 2006 swarm in panel 4 of Fig. 11 (baselines ITOUYAHATANO-ODAWARA and ITOUYAHATANO-HATSUSHIMA), as seen in the leveling survey for benchmark 9338 (red curve in Fig. 10). However, the tendency for relative heights to remain unchanged over time (no increasing nor decreasing trend in relative height) for all of the baselines was generally observed. Combining the results of the leveling survey (Fig. 10) and those of baseline changes (Figs. 11 and 12) shows no significant uplift in the study period (Jan. 2005-Dec. 2020).

Periods of no significant uplift were observed in the study region. A study based on morphology, stratigraphy, and fossil assemblages in the eastern side of the Izu Peninsula (Shishikura et al., 2023)

identified three events over 1500 years: a 1.05-m uplift in 595-715, a 1.33-m uplift in 1356-1666, and a 0.82-m uplift after 1830. The interval between events was 400-800 years. Cumulative uplift of 0.6-0.9 m since 1904, shown in Fig. 10, plus an uplift of 0.1-0.2 m in 1868 or 1870 (Koyama, 1999) before the start of instrument measurement, roughly coincided with the uplift of 0.82 m after 1830 (Shishikura et al., 2023). This last uplift was mainly caused by vertical movement due to subsurface magmatic movement accompanied by earthquake swarms, while the first and second uplifts were considered to be caused by similar volcanic deformation or coseismic deformation due to offshore faults. There existed two periods (715-1356 and 1666-1830) of no uplift during 1500 years in the eastern side of the Izu Peninsula.

## 6. Conclusions

The primary purpose of this study was to better understand the characteristics of the time-dependent activity of LFEs in the Izu-Tobu region during Jan. 2005-Dec. 2020. The output obtained from this study was that relative quiescence occurred and the start of the quiescence roughly coincided with that of ordinary earthquakes. To obtain it, we produced the LFE catalog using the MF method. Then, a first-order timeseries analysis of LFEs during the study period (Jan. 2005-Dec. 2020) was conducted using the standard single ETAS model and an alternative two-stage ETAS model, considering different parameter values in subperiods before and after  $T_c$ . The latter two-stage model was significantly better than the former single model, when  $T_c$  fell in the period mid-2012 to mid-2013 (Figs. 5 and 6). For comparison, the same analysis was conducted for ordinary earthquakes, showing a similar result with  $T_c$  falling in the period of late 2009 to mid-2011. The results of both types of earthquakes indicate that quiescence occurred around the timing of the 2009 and 2011 swarms. Beyond that, we observed that the second-order quiescence occurred before the start of the first-order quiescence. The second-order quiescence started around the timing of the 2006 swarm (Figs. 8 and 9). We associated observed quiescence for both types of earthquakes with a decrease in  $\mu$ , and interpreted it to be directly caused by the magma source.

For a comparison with subsurface seismicity in the Izu-Tobu region, surface vertical displacement data obtained from a leveling survey and the GEONET were used (Figs. 10-12). We observed that the uplift was significant during the 1970s-1990s while it was in abatement or unobservable in the 2000s and later. The quiescence (Figs. 5-9), with no significant crustal movement, is interpreted as an indication that the magma source, which transported magma that intruded into the Izu-Tobu region, was in a transition phase becoming inactive, after having been active during the 1970s-1990s.

Our observation indicating changes in seismicity without crustal deformation at an active volcano area is not a surprise. LFEs beneath the active volcano Mt. Fuji activated after the *M*5.9 Shizuoka earthquake that occurred on Mar. 15, 2011 at the foot of the volcano, and the occurrence rate of LFEs did not return to pre-earthquake levels (Nanjo et al., 2023). No crustal deformation during the *M*5.9 event was reported.

Detailed observations raised a question regarding the earlier start of quiescence for ordinary earthquakes than for LFEs (Figs. 5, 7, and 8). Namely, the timing of the  $T_c$ -value for both types of earthquakes remains unexplained. Being able to answer this question would allow us to move toward a better understanding of how magma source changes with time while offering a better prediction regarding whether the seismicity continues quietly or is activated with/without the occurrence of a swarm. Our future work will be directed at answering this question.

#### **Data availability**

The datasets used and/or analyzed during the current study are available from the corresponding author upon reasonable request. The JMA catalog was obtained from <https://www.data.jma.go.jp/eqev/data/bulletin/hypo.html>. The waveform records were obtained from the permanent stations of the National Research Institute for Earth Science and Disaster Resilience, Earthquake Research Institute at the University of Tokyo, JMA, and the Hot Springs Research Institute of the Kanagawa Prefectural Government. The location of Teishi Knoll, used for Figs. 1 and 2, was obtained from <https://www.mri-jma.go.jp/Dep/sei/fhirose/plate/en.PlateData.html>. The location of the Higashi-Izu JMA station, used for Fig. 1, was obtained from Kumazawa (2016). The seismicity analysis software ZMAP (Wiemer, 2001), used for Fig. 4, was obtained from <http://www.seismo.ethz.ch/en/research-and-teaching/products-software/software/ZMAP>. The program XETAS (Ogata and Tsuruoka, 2016), used for Figs. 5-9, was obtained from <http://evrrss.eri.u-tokyo.ac.jp/software/xetas/index.html>. Data shown in Fig. 10 were reproduced from GSI (2016). Generic Mapping Tools (GMT) (Wessel et al., 2013), used for Figs. 1-3 and 10-12, is an open-source collection (<https://www.generic-mapping-tools.org>). GEONET data (Muramatsu et al., 2021; Takamatsu et al., 2023), used for Figs. 11 and 12, were obtained from <https://mekira.gsi.go.jp/index.en.html>.

#### **CRedit authorship contribution statement**

**K. Z. Nanjo:** Conceptualization, Investigation, Project administration, Formal analysis, Methodology, Software, Validation, Writing-original draft, Writing-review & editing. **Y. Yukutake:**

Conceptualization, Investigation, Data curation, Resources, Writing-review & editing. **T. Kumazawa**: Investigation, Methodology, Software, Writing-review & editing.

### **Declaration of Competing Interests**

The authors declare that they have no known competing financial interests or personal relationships that could have appeared to influence the work reported in this paper.

### **Acknowledgments**

This study was partially supported by the Ministry of Education, Culture, Sports, Science and Technology (MEXT) of Japan, under The Second Earthquake and Volcano Hazards Observation and Research Program (Earthquake and Volcano Hazard Reduction Research) (K.Z.N., Y.Y.) and under STAR-E (Seismology TowArD Research innovation with data of Earthquake) Program Grant Number JPJ010217 (K.Z.N., T.K.), JSPS KAKENHI Grant Numbers JP 22K03752 (Y.Y.), 20K11704 (T.K.), and a Research Grant of the Izu Peninsula UNESCO Global Geopark (K.Z.N., Y.Y.). The authors thank Y. Noda for help with implementing the MF method.

### **References**

- Akaike, H., 1974. A new look at the statistical model identification. *IEEE Transactions on Automatic Control* 19(6), 716-723. <https://doi.org/10.1109/TAC.1974.1100705>.
- Aso, N., Ohta, K., Ide, S., 2013. Tectonic, volcanic, and semi-volcanic deep low-frequency earthquakes in western Japan. *Tectonophysics* 600, 27-40. <https://doi.org/10.1016/j.tecto.2012.12.015>.
- Aramaki, S., Hamuro, K., 1977. Geology of the Higashi-Izu monogenetic volcano group. *Bulletin of the Earthquake Research Institute, University of Tokyo* 52, 235-278 (in Japanese with English abstract). <https://doi.org/10.15083/0000033207>.
- Brodsky, E.E., Lajoie, L.J., 2013. Anthropogenic seismicity rates and operational parameters at the Salton Sea geothermal field. *Science* 341(6145), 543-546. <https://doi.org/10.1126/science.1239213>.
- Delahaye, E.J., Townend, J., Reyners, M.E., Rogers, G., 2009. Microseismicity but no tremor accompanying slow slip in the Hikurangi subduction zone, New Zealand. *Earth and Planetary Science Letters* 277(1-2), 21-28. <https://doi.org/10.1016/j.epsl.2008.09.038>.

- Dieterich, J., Cayol, V., Okubo, P.G., 2000. The use of earthquake rate changes as a stress meter at Kilauea volcano. *Nature* 408, 457-460. <https://doi.org/10.1038/35044054>.
- Earthquake Research Committee, 2010. Prediction methods of Izu eastern seismic activity. The Headquarters for Earthquake Research Promotion, Ministry of Education, Culture and Sport, Science and Technology (MEXT), Japan (in Japanese). <http://www.jishin.go.jp/main/yosoku/izu/index.htm> (Last accessed on Dec. 27, 2024).
- Einarsson, P., Brandsdottir, B., 1980. Seismological evidence for lateral magma intrusion during the July 1978 deflation of the Krafla volcano in NE Iceland. *Journal of Geophysics* 47(1), 160-165. <https://journal.geophysicsjournal.com/JofG/article/view/134>.
- Feuillet, N., Nostro, C., Chiarabba, C., Cocco, M., 2004. Coupling between earthquake swarms and volcanic unrest at the Alban Hills Volcano (central Italy) modeled through elastic stress transfer. *Journal of Geophysical Research* 109, B02308. <https://doi.org/10.1029/2003JB002419>.
- Geospatial Information Authority of Japan, 2016. Crustal movements in the Izu peninsula and its vicinity. Report of the Coordinating Committee for Earthquake Prediction, Japan 96, 144-163 (in Japanese). [https://cais.gsi.go.jp/YOCHIREN/report/kaihou96/05\\_01.pdf](https://cais.gsi.go.jp/YOCHIREN/report/kaihou96/05_01.pdf) (Last accessed on Dec. 27, 2024).
- Green, D.N., Neuberg, J., 2006. Waveform classification of volcanic low-frequency earthquake swarms and its implication at Soufrière Hills Volcano, Montserrat. *Journal of Volcanology and Geothermal Research* 153(1-2), 51-63. <https://doi.org/10.1016/j.jvolgeores.2005.08.003>.
- Gutenberg, B., Richter, C.F. 1944. Frequency of earthquakes in California. *Bulletin of the Seismological Society of America* 34(4), 185-188. <https://doi.org/10.1785/BSSA0340040185>.
- Hainzl, S., Ogata, Y., 2005. Detecting fluid signals in seismicity data through statistical earthquake modeling. *Journal of Geophysical Research* 110(B5), B05S07. <https://doi.org/10.1029/2004JB003247>.
- Hayashi, Y., Morita, Y., 2003. An image of a magma intrusion process inferred from precise hypocentral migrations of the earthquake swarm east off the Izu Peninsula. *Geophysical Journal International* 153(1), 159-174. <https://doi.org/10.1046/j.1365-246X.2003.01892.x>.
- Ishida, M., 1984. Spatial-temporal variation of seismicity and spectrum of the 1980 earthquake swarm near the Izu Peninsula, Japan. *Bulletin of the Seismological Society of America* 74(1), 199-221. <https://doi.org/10.1785/BSSA0740010199>.



- Kato, A., Obara, K., Igarashi, T., Tsuruoka, H., Nakagawa, S., Hirata, N., 2012. Propagation of slow slip leading up to the 2011 Mw 9.0 Tohoku-Oki earthquake. *Science* 335, 705-708.  
<https://doi.org/10.1126/science.1215141>.
- Koyama, M., 1999. Pre-20th century of earthquake swarms and volcanic activity in the Higashi Izu monogenetic volcano field, based on historical documents. *The Quaternary Research (Daiyonki-Kenkyu)* 38(6), 435-446 (in Japanese with English abstract).  
<https://doi.org/10.4116/jaqua.38.435>.
- Koyama, M., Umino, S., 1991. Why does the Higashi-Izu monogenetic volcano group exist in the Izu Peninsula? Relationships between late Quaternary volcanism and tectonics in the northern tip of the Izu-Bonin arc. *Journal of Physics of the Earth* 39(1), 391-420.  
<https://doi.org/10.4294/jpe1952.39.391>.
- Kumazawa, T., Ogata, Y., Kimura, K., Maeda, K., Kobayashi, A., 2016. Background rates of swarm earthquakes that are synchronized with volumetric strain changes. *Earth and Planetary Science Letters* 442, 51-60. <https://doi.org/10.1016/j.epsl.2016.02.049>.
- Kumazawa, T., Ogata, Y., Toda, S., 2010. Precursory seismic anomalies and transient crustal deformation prior to the 2008 Mw = 6.9 Iwate-Miyagi Nairiku, Japan, earthquake. *Journal of Geophysical Research* 115, B10312. <https://doi.org/10.1029/2010JB007567>.
- Kumazawa, T., Ogata, Y., Tsuruoka, H., 2019. Characteristics of seismic activity before and after the 2018 M6.7 Hokkaido Eastern Iburi earthquake. *Earth, Planets and Space* 71, 130.  
<https://doi.org/10.1186/s40623-019-1102-y>.
- Kurihara, R., Obara, K. 2021. Spatiotemporal characteristics of relocated deep low-frequency earthquakes beneath 52 volcanic regions in Japan over an analysis period of 14 years and 9 months. *Journal of Geophysical Research* 126(10), e2021JB022173.  
<https://doi.org/10.1029/2021JB022173>.
- Lamb, O.D., De Angelis, S., Umakoshi, K., Hornby, A.J., Kendrick, J.E., Lavallée, Y., 2015. Repetitive fracturing during spine extrusion at Unzen volcano, Japan. *Solid Earth* 6, 1,277-1,293.  
<https://doi.org/10.5194/se-6-1277-2015>.
- Lei, X., Yu, G., Ma, S., Wen, X., Wang, Q., 2008. Earthquakes induced by water injection at ~3 km depth within the Rongchang gas field, Chongqing, China. *Journal of Geophysical Research* 113(B10), B10310. <https://doi.org/10.1029/2008JB005604>.

- Llenos, A.L., McGuire, J.J., 2011. Detecting aseismic strain transients from seismicity data. *Journal of Geophysical Research* 116, B06305. <https://doi.org/10.1029/2010JB007537>.
- Llenos, A.L., McGuire, J.J., Ogata, Y., 2009. Modeling seismic swarms triggered by aseismic transients. *Earth and Planetary Science Letters* 281(1-2), 59-69. <https://doi.org/10.1016/j.epsl.2009.02.011>.
- Miyamura, J., Ueno, H., Yokota, T., 2010. Estimation of amount of intrusive magma by using volumetric strain data and attempt of evaluation of volcanic activity in Izu-Tobu volcanoes. *Geophysical bulletin of Hokkaido University* 73, 239-255. <http://doi.org/10.14943/gbhu.73.239>.
- Morita, Y., Nakao, S., Hayashi, Y., 2006. A quantitative approach to the dike intrusion process inferred from a joint analysis of geodetic and seismological data for the 1998 earthquake swarm off the east coast of Izu Peninsula. *Journal of Geophysical Research* 111, B06208. <https://doi.org/10.1029/2005JB003860>.
- Muramatsu, H., Takamatsu, N., Abe, S., Furuya T., Kato C., Ohno, K., Hatanaka, Y., Kakiage, Y., Ohashi, K., 2021. Updating daily solution of CORS in Japan using new GEONET 5th analysis strategy. *Journal of the Geospatial Information Authority of Japan* 134, 19-32 (in Japanese). [https://doi.org/10.57499/JOURNAL\\_134\\_03](https://doi.org/10.57499/JOURNAL_134_03).
- Nagamune, T., Yokoyama, H., Fukudome, A., 1992. Earthquake swarms off the east coast of the Izu peninsula and their relation to the 1989 eruption of Teishi Knoll volcano. *Kazan (Bulletin of the volcanological Society of Japan)* 37(1), 1-8 (in Japanese with English abstract). [https://doi.org/10.18940/kazan.37.1\\_1](https://doi.org/10.18940/kazan.37.1_1).
- Nanjo, K.Z., 2020. Were changes in stress state responsible for the 2019 Ridgecrest, California, earthquakes? *Nature Communications* 11, 3082. <https://doi.org/10.1038/s41467-020-16867-5>.
- Nanjo, K.Z., Yoshida, A. 2018. A *b* map implying the first eastern rupture of the Nankai Trough earthquakes. *Nature Communications* 9(1), 1117. <https://doi.org/10.1038/s41467-018-03514-3>.
- Nanjo, K.Z., Yukutake, Y., Kumazawa, T., 2023. Activated volcanism of Mount Fuji by the 2011 Japanese large earthquakes. *Scientific Reports* 13, 10562. <https://doi.org/10.1038/s41598-023-37735-4>.
- Obara, K., 2002. Nonvolcanic deep tremor associated with subduction in southwest Japan. *Science* 296(5573), 1679-1681. <https://doi.org/10.1126/science.1070378>.

- Ogata, Y., 1988. Statistical models for earthquake occurrences and residual analysis for point processes. *Journal of the American Statistical Association* 83, 9-27.  
<https://doi.org/10.2307/2288914>.
- Ogata, Y., 1992. Detection of precursory relative quiescence before great earthquakes through a statistical model. *Journal of Geophysical Research* 97, 19845-19871.  
<https://doi.org/10.1029/92JB00708>.
- Ogata, Y., Tsuruoka, H., 2016. Statistical monitoring of aftershock sequences: a case study of the 2015 Mw7.8 Gorkha, Nepal, earthquake. *Earth, Planets and Space* 68, 44.  
<https://doi.org/10.1186/s40623-016-0410-8>.
- Okada, Y., Yamamoto, E., 1991. Dyke intrusion model for the 1989 seismovolcanic activity off Ito, Central Japan. *Journal of Geophysical Research* 96(B6), 10361-10376.  
<https://doi.org/10.1029/91JB00427>.
- Okada, Y., Yamamoto, E., Ohkubo T., 2000. Coswarm and preswarm crustal deformation in the eastern Izu Peninsula, central Japan. *Journal of Geophysical Research* 105(B1), 681-692.  
<https://doi.org/10.1029/1999JB900335>.
- Ozawa, S., Miyazaki, S., Hatanaka, Y., Imakiire, T., Kaidzu, M., Murakami, M., 2003. Characteristic silent earthquakes in the eastern part of the Boso peninsula, Central Japan. *Geophysical Research Letters* 30(6), 1283. <https://doi.org/10.1029/2002GL016665>.
- Peng, Z., Zhao, P., 2009. Migration of early aftershocks following the 2004 Parkfield earthquake. *Nature Geoscience* 2, 877-881. <https://doi.org/10.1038/ngeo697>.
- Petersen, T., 2007. Swarms of repeating long-period earthquakes at Shishaldin Volcano, Alaska, 2001-2004. *Journal of Volcanology and Geothermal Research* 166(3-4), 177-192.  
<https://doi.org/10.1016/j.jvolgeores.2007.07.014>.
- Ross, Z.E., Idini, B., Jia, Z., Stephenson, O.L., Zhong, M., Wang, X., Zhan, Z., Simons, M., Fielding, E.J., Yun, S.-H., Hauksson, E., Moore, A.W., Liu, Z., Jung, J., 2019. Hierarchical interlocked orthogonal faulting in the 2019 Ridgecrest earthquake sequence. *Science* 366(6463), 346-351.  
<https://doi.org/10.1126/science.aaz0109>.
- Schorlemmer, D., Neri, G., Wiemer, S., Mostaccio, A., 2003. Stability and significance tests for *b*-value anomalies: example from the Tyrrhenian Sea. *Geophysical Research Letters* 30(16), 1835.  
<https://doi.org/10.1029/2003GL017335>.

- Segall, P., Desmarais, E.K., Shelly, D., Miklius, A., Cervelli, P., 2006. Earthquakes triggered by silent slip events of Kilauea volcano, Hawaii. *Nature* 442, 71-74. <https://doi.org/10.1038/nature04938>.
- Shelly, D.R., Beroza, G.C., Ide, S., 2007. Non-volcanic tremor and low-frequency earthquake swarms. *Nature* 446, 305-307. <https://doi.org/10.1038/nature05666>.
- Shimazaki, K., 1988. Dyke intrusion hypothesis at east off Izu Peninsula. Abstracts, vol. 1, p. 330, Seismological Society of Japan, Tokyo (in Japanese).
- Shishikura, M., Namegaya, Y., Kaneko, H., Koyama, M., 2023. Late Holocene tectonics inferred from emerged shoreline features in Higashi-Izu monogenetic volcano field, Central Japan. *Tectonophysics* 864, 229985. <https://doi.org/10.1016/j.tecto.2023.229985>.
- Smith, K.D., von Seggern, D., Blewitt, G., Preston, L., Anderson, J.G., Wernicke, B.P., Davis, J.L., 2004. Evidence for deep magma injection beneath Lake Tahoe, Nevada-California. *Science* 305(5688), 1277-1280. <https://doi.org/10.1126/science.1101304>.
- Tada, T., Hashimoto, M., 1989. On the cause of abnormal crustal deformation in the northeastern Izu Peninsula 3, Open crack model and activity in the summer of 1988, Abstracts, vol. 1, p. 41, Seismological Society of Japan, Tokyo (in Japanese).
- Takamatsu, N., Muramatsu, H., Abe, S., Hatanaka, Y., Furuya, T., Kakiage, Y., Ohashi, K., Kato, C., Ohno, K., Kawamoto, S., 2023. New GEONET analysis strategy at GSI: daily coordinates of over 1300 GNSS CORS in Japan throughout the last quarter century. *Earth, Planets and Space* 75, 49. <https://doi.org/10.1186/s40623-023-01787-7>.
- Terakawa, T., 2014. Evolution of pore fluid pressures in a stimulated geothermal reservoir inferred from earthquake focal mechanisms. *Geophysical Research Letters* 41(21), 7468-7476. <https://doi.org/10.1002/2014GL061908>.
- Terakawa, T., Hashimoto, C., Matsu'ura, M., 2013. Changes in seismic activity following the 2011 Tohoku-oki Earthquake: effects of pore fluid pressure. *Earth and Planetary Science Letters* 365, 17-24. <https://doi.org/10.1016/j.epsl.2013.01.017>.
- Toda, S., Stein, R., Sagiya, T., 2002. Evidence from the A.D. 2000 Izu Islands swarm that seismicity is governed by stressing rate. *Nature* 419, 58-61. <https://doi.org/10.1038/nature00997>.
- Ukawa, M., 1991. Collision and fan-shaped compressional stress pattern in the Izu block at the northern edge of the Philippine Sea plate. *Journal of Geophysical Research* 96(B1), 713-728. <https://doi.org/10.1029/90JB02142>.

- Wessel, P., Smith, W.H.F., Scharroo, R., Luis, J.F., Wobbe, F., 2013. Generic Mapping Tools: improved version released. *EOS, Transactions, AGU* 94(45), 409-410.  
<https://doi.org/10.1002/2013EO450001>.
- Wiemer, S., 2001. A software package to analyze seismicity: ZMAP. *Seismological Research Letters* 72(3), 373-382. <https://doi.org/10.1785/gssrl.72.3.373>.
- Waite, G.P., Smith, R.B., 2002. Seismic evidence for fluid migration accompanying subsidence of the Yellowstone caldera. *Journal of Geophysical Research* 107(B9), 2177.  
<https://doi.org/10.1029/2001JB000586>.
- Woessner, J., Wiemer, S., 2005. Assessing the quality of earthquake catalogues: estimating the magnitude of completeness and its uncertainty. *Bulletin of the Seismological Society of America* 95, 684-698. <https://doi.org/10.1785/0120040007>.
- Yamamoto, T., Soya, T., Suto, S., Uto, K., Takada, A., Sakaguchi, K., Ono, K., 1991. The 1989 submarine eruption off eastern Izu Peninsula, Japan: ejecta and eruption mechanisms. *Bulletin of Volcanology* 53, 301-308. <https://doi.org/10.1007/BF00414526>.
- Yukutake, Y., 2017. Development of a routine system for a deep-low frequency earthquake in Hakone Volcano, by using the matched filter method. *Bulletin of the Hot Springs Research Institute of Kanagawa Prefecture* 49, 1-10 (in Japanese with English abstract).  
[https://www.onken.odawara.kanagawa.jp/files/PDF/houkoku/49/houkoku49\\_p01-10.pdf](https://www.onken.odawara.kanagawa.jp/files/PDF/houkoku/49/houkoku49_p01-10.pdf).
- Yukutake, Y., Abe, Y., Doke, R. 2019. Deep low-frequency earthquakes beneath the Hakone volcano, central Japan, and their relation to volcanic activity. *Geophysical Research Letters* 46(20), 11035-11043. <https://doi.org/10.1029/2019GL084357>.

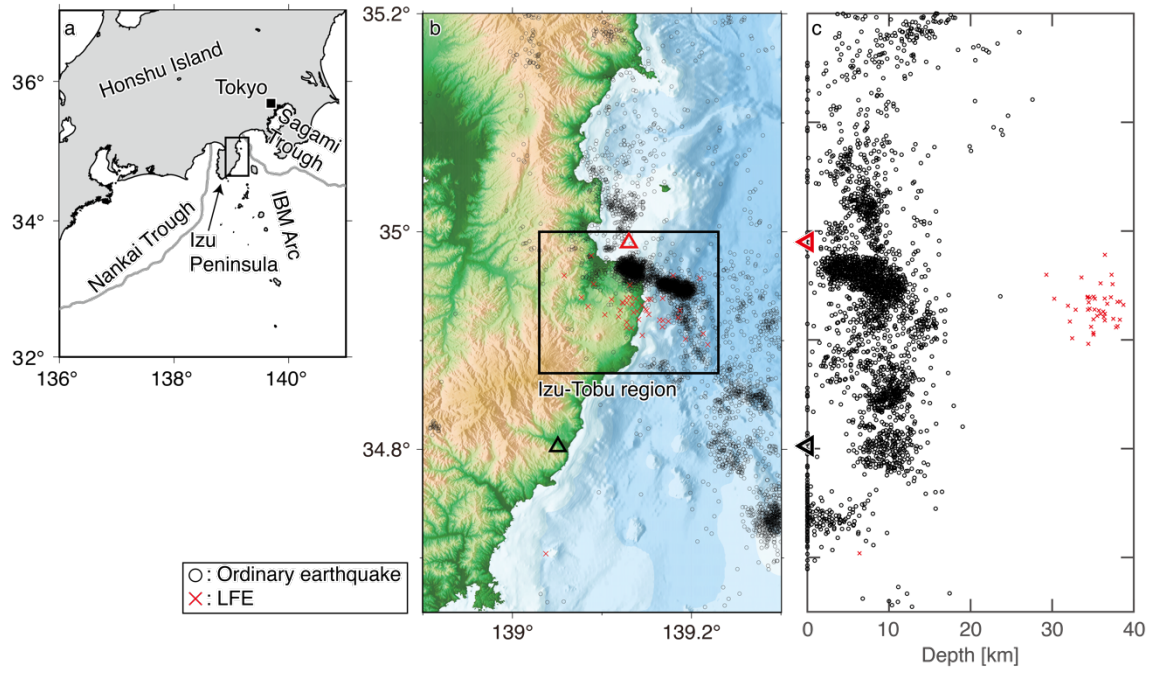


**Fig. 1.** Seismicity in and around the study region. **a**, Central Japan including the region (black rectangle) of **b**. Gray curves indicate trough axes. IBM Arc: Izu-Bonin-Mariana Arc. **b**, Map showing ordinary earthquakes with  $M \geq 1$  (black circle) and LFEs with  $M \geq 0.1$  (red cross) at depths 0-40 km during the period Jan. 2005-Dec. 2020. To plot these earthquakes, the JMA catalog was used. Red triangle indicates the Teishi Knoll. Black rectangle indicates the study region called the Izu-Tobu region. Black triangle indicates the Higashi-Izu JMA station, at which a strainmeter that recorded volumetric strain data used by Kumazawa et al. (2016) was installed. **c**, Cross-sectional view of ordinary earthquakes and LFEs.

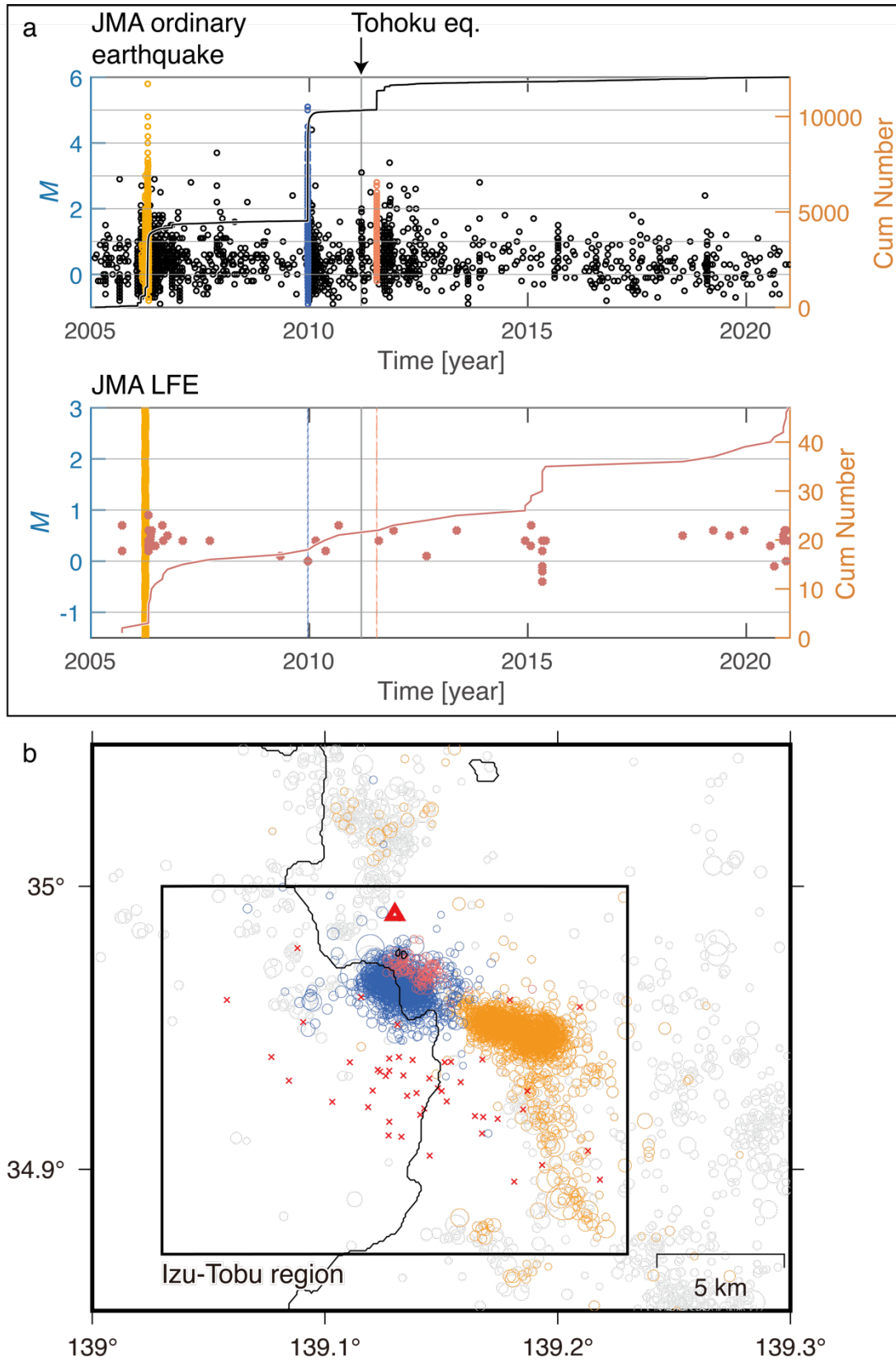


**Fig. 2.** Space-time distribution of earthquakes in the Izu-Tobu region. **a**, Top panel:  $M$ -time diagram (y-axis on the left side) of ordinary earthquakes (depths of 0-40 km) in the study region indicated by a

black rectangle in **b**. These earthquakes were obtained from the JMA catalog. Overlapped is the cumulative number of ordinary earthquakes as a function of time (y-axis on the right side). Three abrupt increases in the cumulative number of ordinary earthquakes indicate three earthquake swarms. Based on GSI (2016), earthquakes in the periods Mar. 1-Apr. 30, 2006 (orange), Dec. 17-21, 2009 (blue), and Jul. 17-18, 2011 (pink) were considered as the 2006, 2009, and 2011 swarms, respectively. Vertical line indicates the moment of the Mar. 11, 2011  $M_9$  Tohoku earthquake. Bottom panel: Same as the top panel for LFEs. Orange, blue, and pink vertical lines indicate the 2006, 2009, and 2011 swarms, respectively. **b**, Map showing ordinary earthquakes (circle) and LFEs (cross) in and around the study region (black rectangle). Earthquakes with  $M \geq 1$  (depths of 0-40 km) in orange, blue, and pink, are the 2006, 2009, and 2011 swarms, respectively. Other ordinary earthquakes are indicated by grey circles. Triangle indicates the Teishi Knoll.



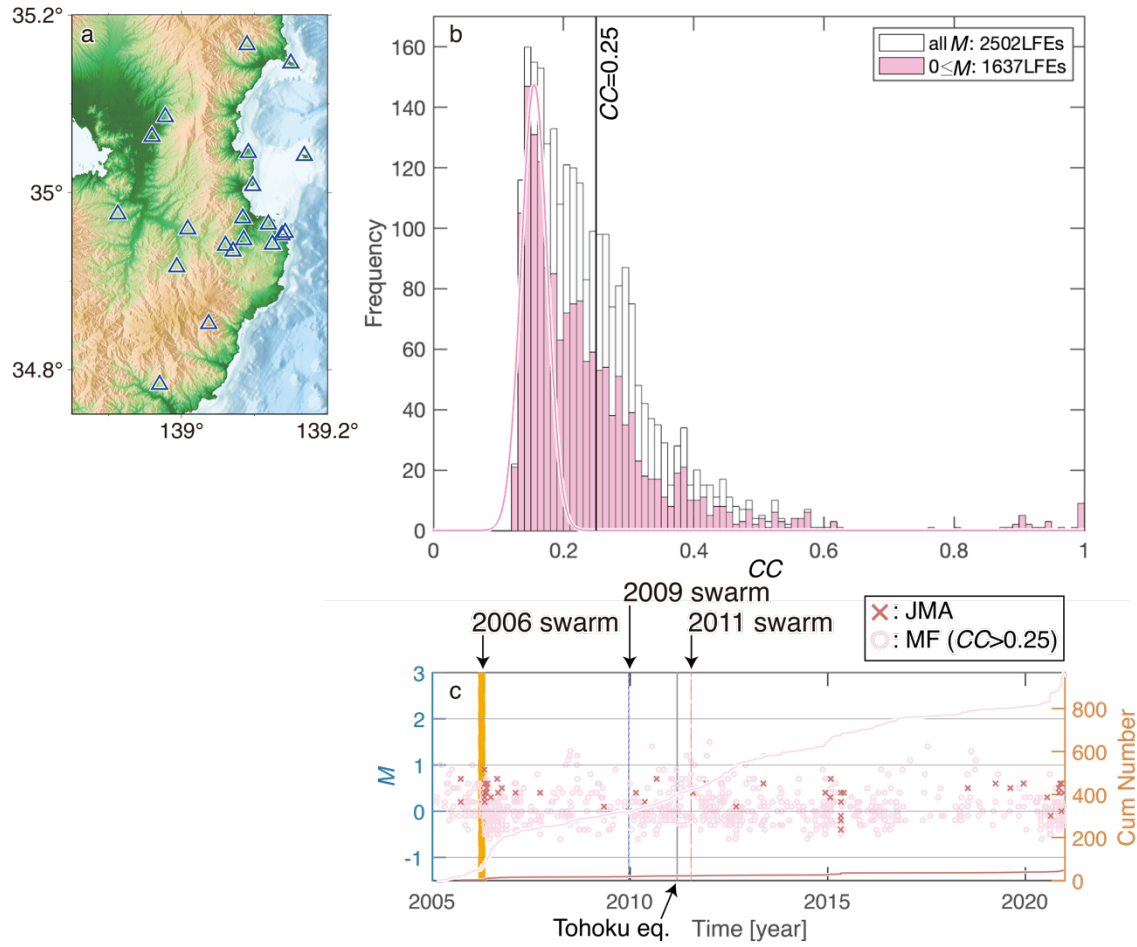


**Fig. 3.** LFEs detected by the MF method. **a**, Stations that recorded waveforms used in this study. **b**, Multiple histograms of  $CC$ -values for all magnitudes (white) and  $M \geq 0$  (pink). Also included is the normally distributed curve (mean of 0.155 and standard deviation of 0.02). Vertical line indicates  $CC=0.25$ . **c**, Same as the bottom panel of Fig. 2a, but data from the MF catalog ( $CC > 0.25$ ) are included, as shown in pink.

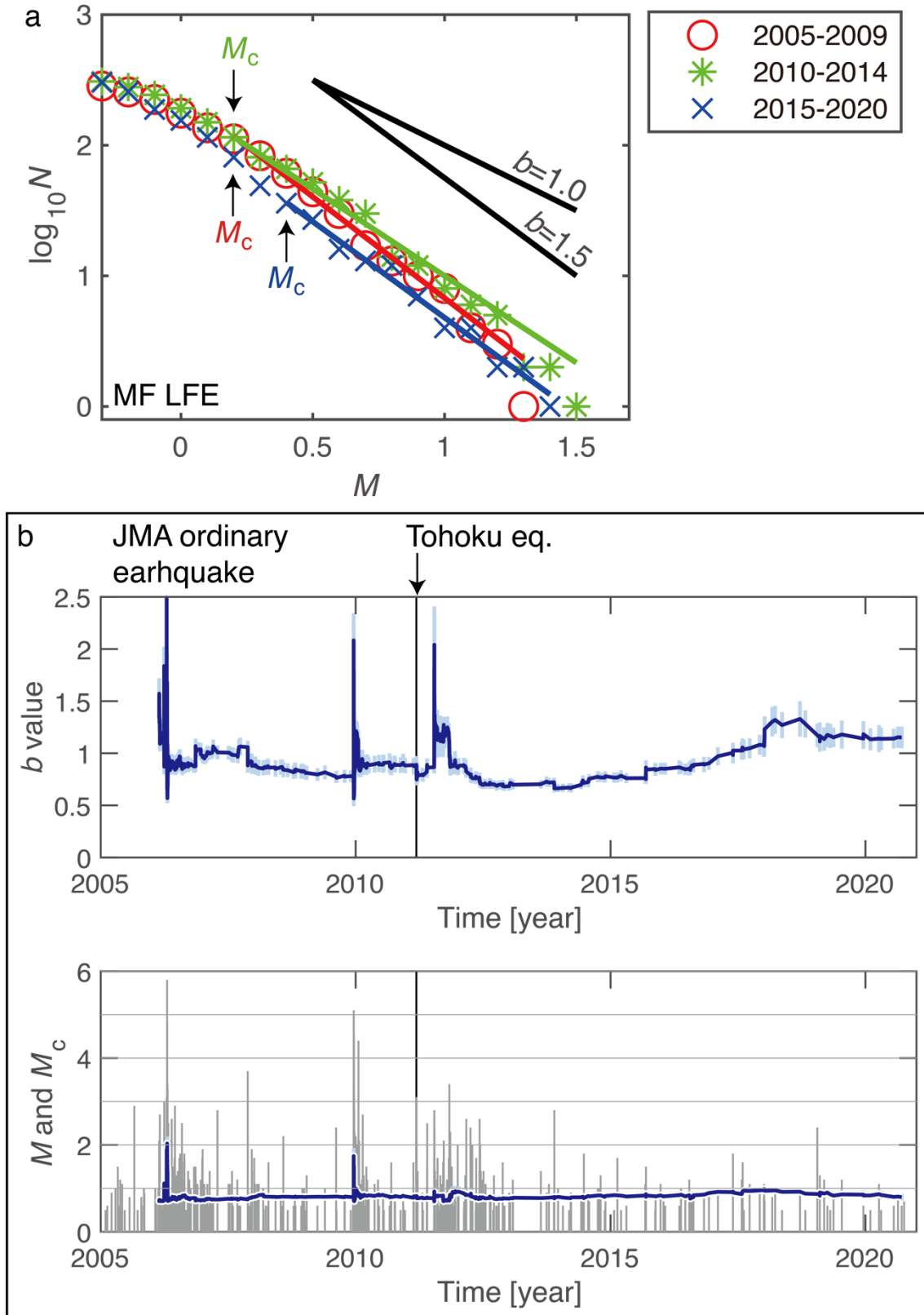


**Fig. 4.**  $M_c$  of LFEs and ordinary earthquakes. **a**, The MF catalog ( $CC > 0.25$ ) was used. Straight lines show the GR law with parameters  $(b, a, M_c) = (1.55, 2.38, 0.2)$  for 2005-2009,  $(1.33, 2.33, 0.2)$  for

2010-2014, and (1.47, 2.15, 0.4) for 2015-2020. **b**, JMA catalog was used. Top panel:  $b$ -value as a function of time. Bottom panel:  $M$  and  $M_c$  as a function of time.

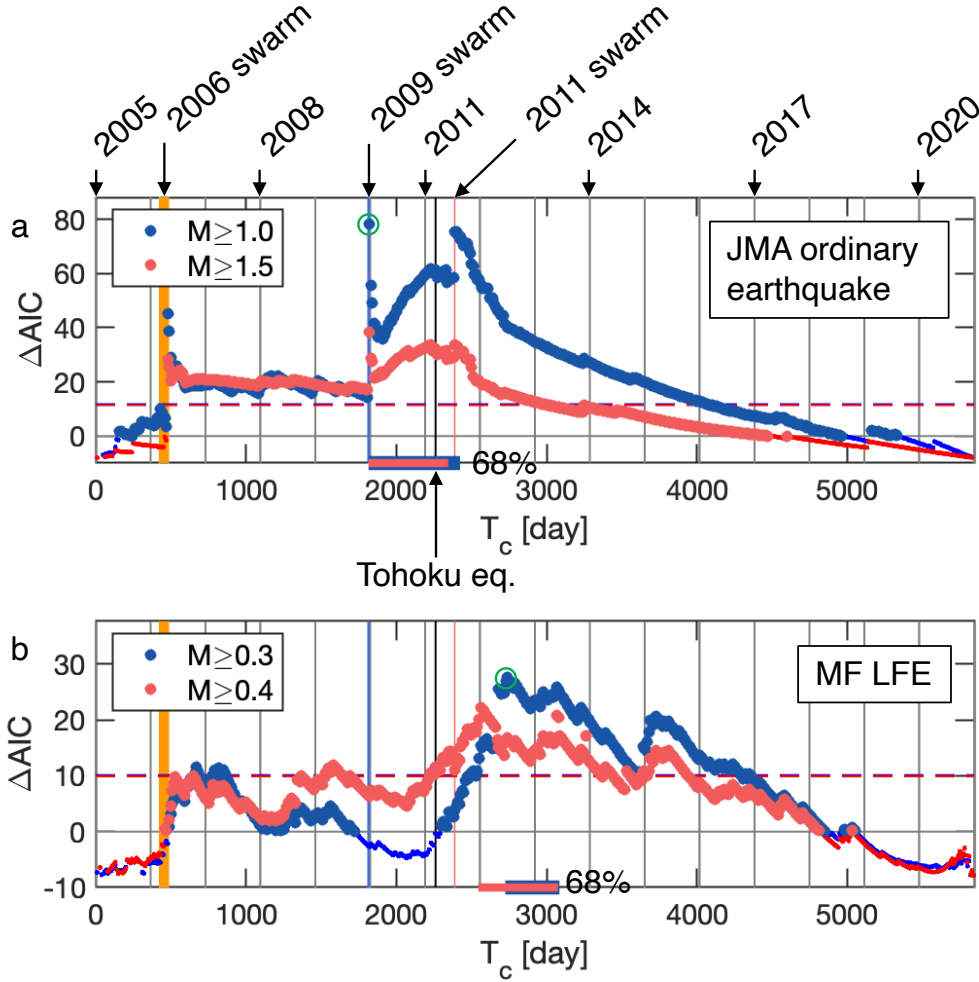


**Fig. 5.** First-order timeseries analysis. **a**,  $\Delta AIC$  as a function of  $T_c$  is shown taking  $M_{th}=1.0$  (blue data) and  $M_{th}=1.5$  (red data) from the JMA catalog of ordinary earthquakes. Small points show that the model-fitting analysis did not converge when assuming the corresponding  $T_c$ . As a reference, grey vertical lines indicate Jan. 1 for 2006–2020. Orange, blue, and pink vertical lines indicate the moment of the 2006, 2009, and 2011 swarms, respectively. Horizontal dashed lines representing  $2q$  for  $M_{th}=1.0$  (blue) and  $M_{th}=1.5$  (red) overlap. The blue horizontal bar represents the change points' confidence interval of 68% (top bar) for  $M_{th}=1.0$ . The red horizontal bar is the same as the blue bar for  $M_{th}=1.5$ . The ETAS fitting for the data point indicated by a green circle is shown in Fig. 6. **b**, Same as **a** for the MF catalog ( $CC>0.25$ ) of LFEs with  $M_{th}=0.3$  (blue) and  $M_{th}=0.4$  (red).

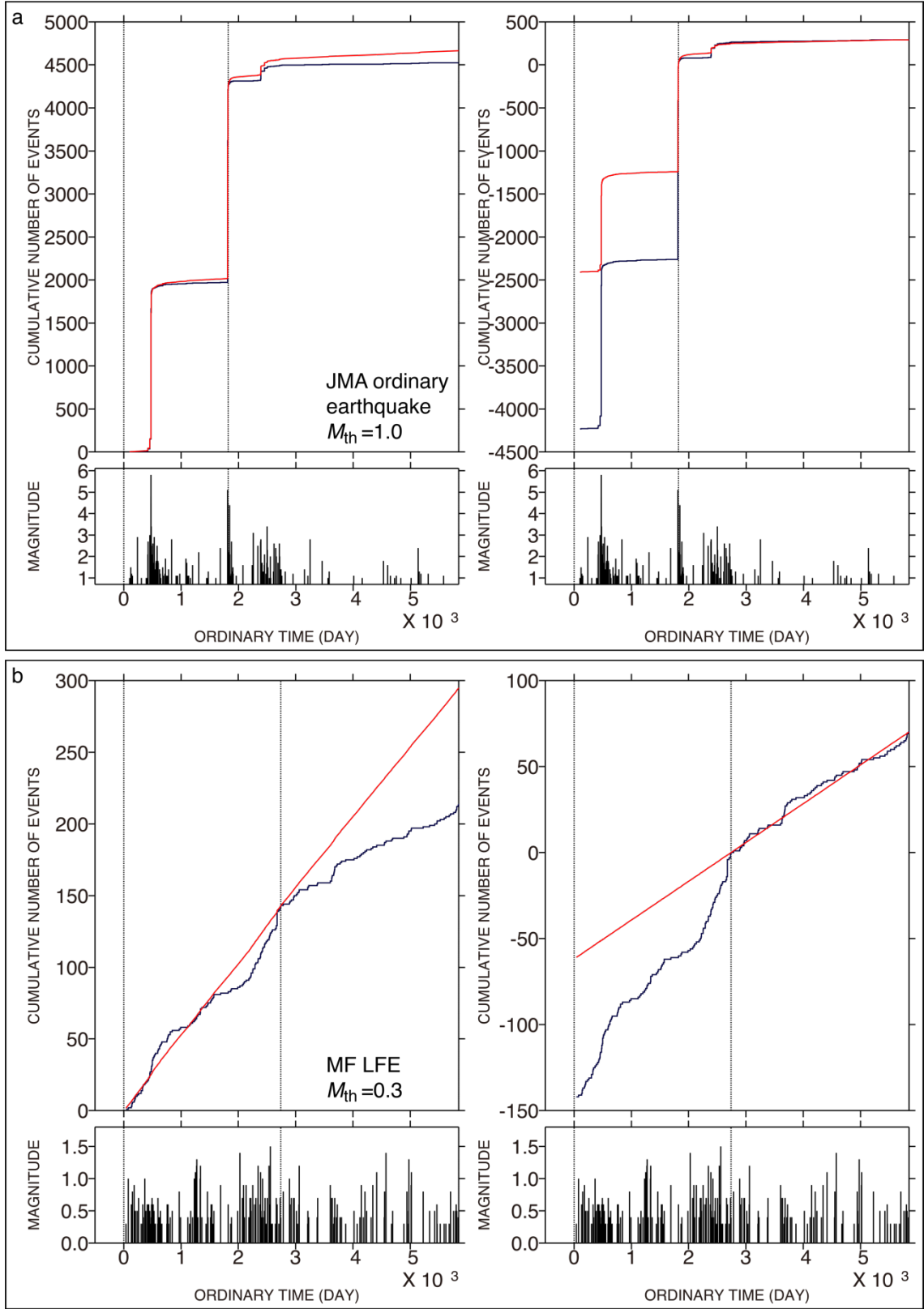


**Fig. 6.** Change point analysis for the first-order timeseries analysis. **a**, Left panel: Cumulative function of  $M \geq 1.0$  for ordinary earthquakes (black curve) is plotted against ordinary time, showing the ETAS

fitting (red curve) in the target interval from Jan. 2005 (first vertical line) until  $T_c=1820$  days (second vertical line) (green circle in Fig. 5a), and then extrapolated until Dec. 2020. Right panel: As in the left panel except that the target is the later time interval after  $T_c=1820$  days. Below these panels, the same  $M$ -time diagram is shown. The ETAS parameters are  $\theta=(\mu, K_0, c, \alpha, p)=(0.019, 0.032, 0.001, 0.058, 1.40)$  for the left panel and  $(0.003, 0.024, 0.001, 0.000, 1.27)$  for the right panel, where the parameters are defined in Kumazawa et al. (2019). **b**, As in **a** except for LFEs ( $M \geq 0.3$ ) and  $T_c=2740$  days (green circle in Fig. 5b).  $\theta=(0.046, 0.00035, 0.001, 0.00, 1.80)$  for the left panel and  $(0.023, 0.00000, 0.001, 0.00, 1.58)$  for the right panel.

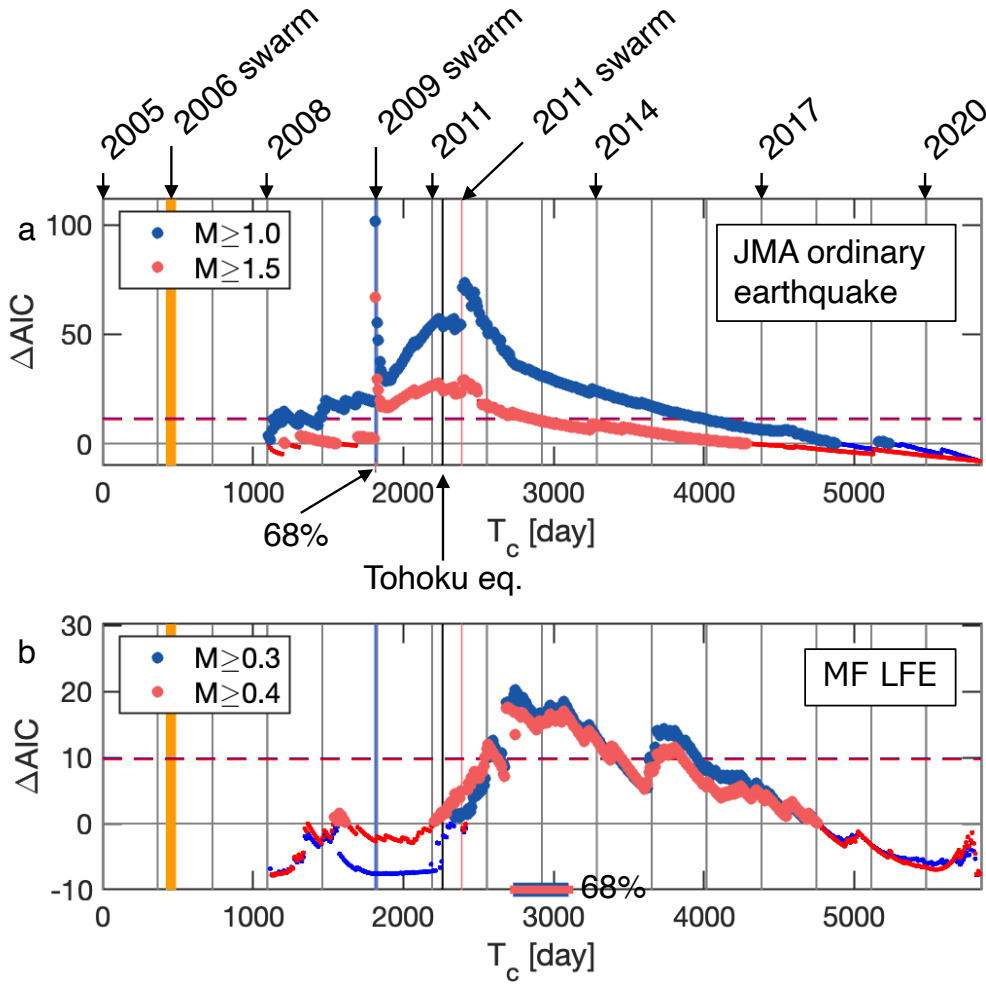


**Fig. 7.** Same as Fig. 5 for seismicity since Jan. 2008.

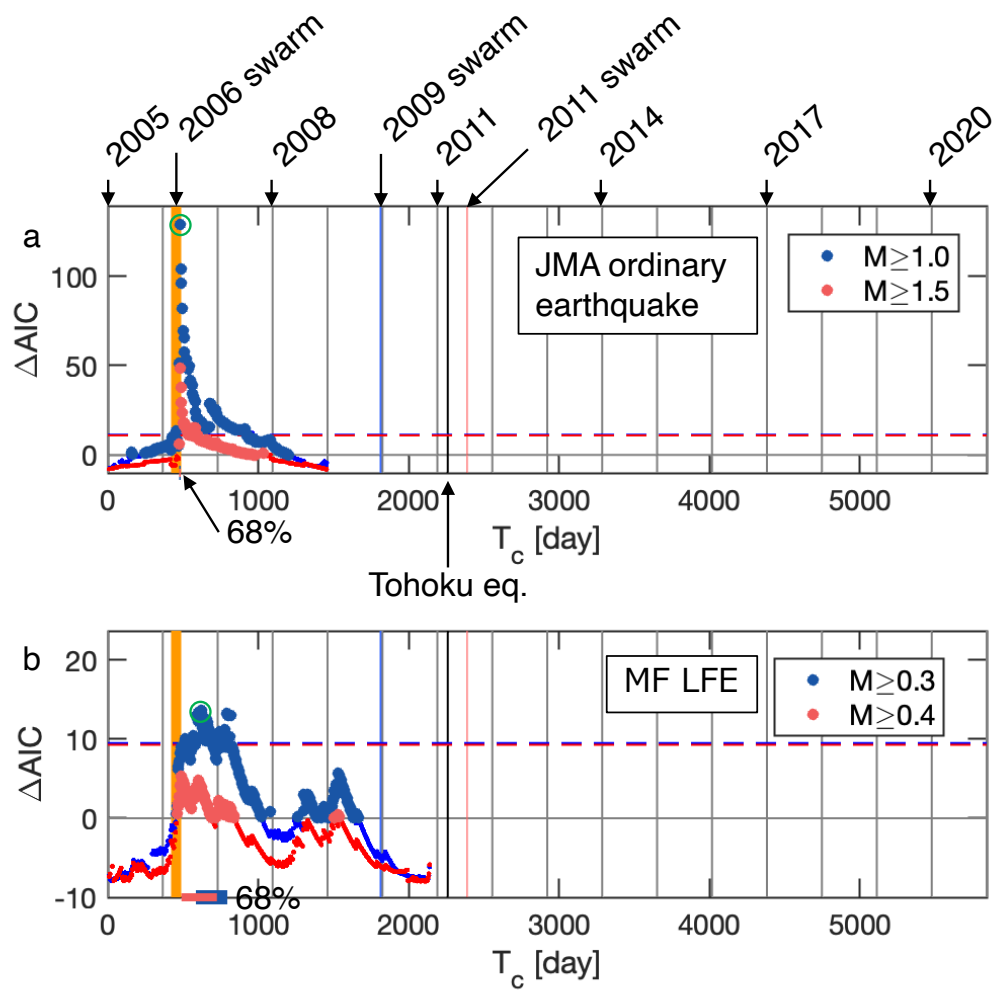


**Fig. 8.** Same as Fig. 5 for the second-order timeseries analysis.

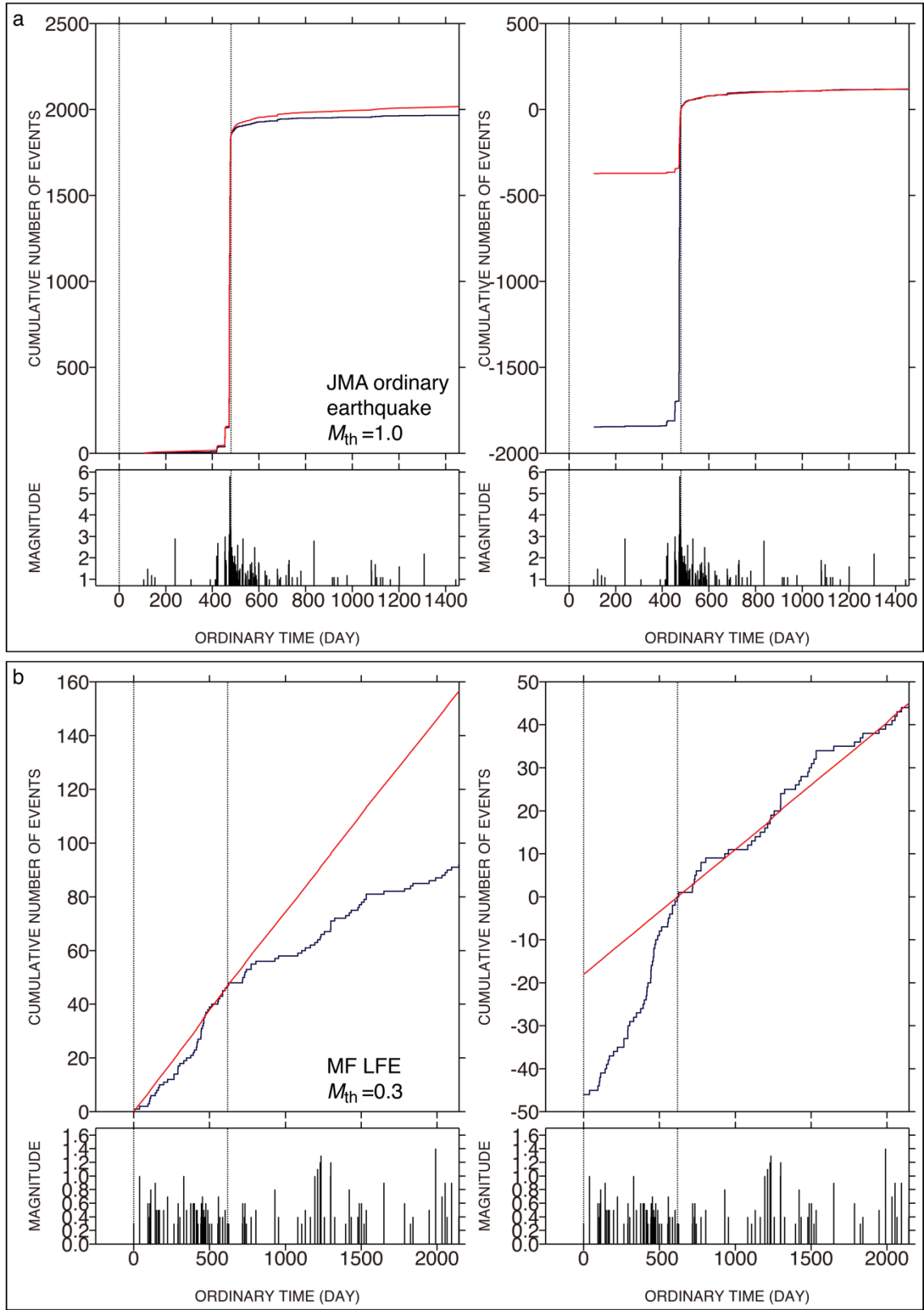


**Fig. 9.** Same as Fig. 6 for second-order timeseries analysis. **a**, Left panel: Cumulative function of  $M \geq 1.0$  for ordinary earthquakes (black curve) is plotted against ordinary time, showing the ETAS

fitting (red curve) in the target interval from Jan. 2005 (first vertical dashed line) until  $T_c=480$  days (second vertical dashed line) (green circle in Fig. 8a), and then extrapolated until Dec. 2008. Right panel: As in the left panel except that the target is the later time interval after  $T_c=480$  days. The ETAS parameters (Kumazawa et al., 2019) are  $\theta=(\mu, K_0, c, \alpha, p)=(0.024, 0.03, 0.001, 0.14, 1.47)$  for the left panel and  $(0.010, 0.07, 0.001, 0.34, 1.12)$  for the right panel. **b**, As in **a** except for LFEs with  $M \geq 0.3$ . The ETAS model was fitted to the target interval from Jan. 2005 until immediately before  $T_c=620$  days (green circle in Fig. 8b), and then extrapolated until Dec. 2010.  $\theta=(0.069, 0.00014, 0.001, 0.00, 1.91)$  for the left panel and  $(0.029, 0.00000, 0.001, 5.69, 4.51)$  for the right panel.



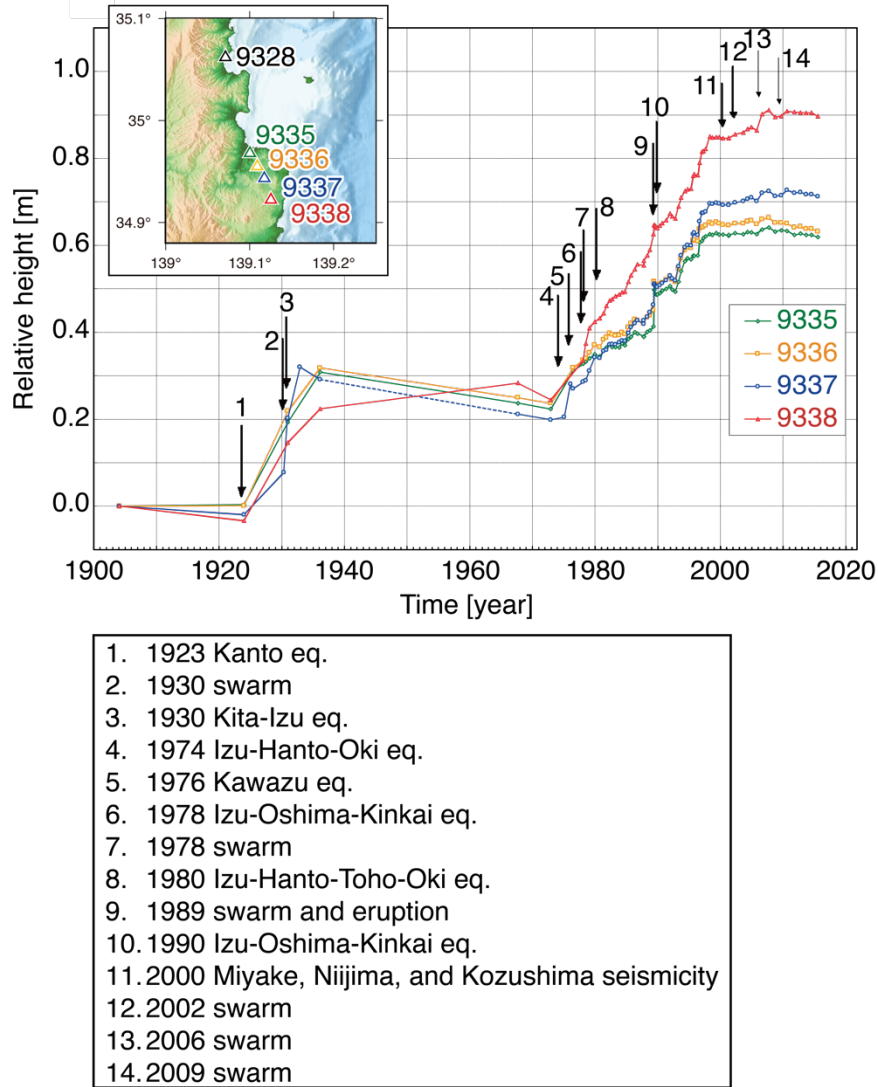


**Fig. 10.** Timeseries of vertical crustal movement. The leveling survey refers to benchmark 9328. Taking the year 1904 as the reference time, the results were obtained by the leveling survey at benchmarks 9335, 9336, 9337, and 9338, whose locations are mapped in the inset. Data points and arrows in the figure were reproduced from GSI (2016). Inset shows the locations of the benchmarks.

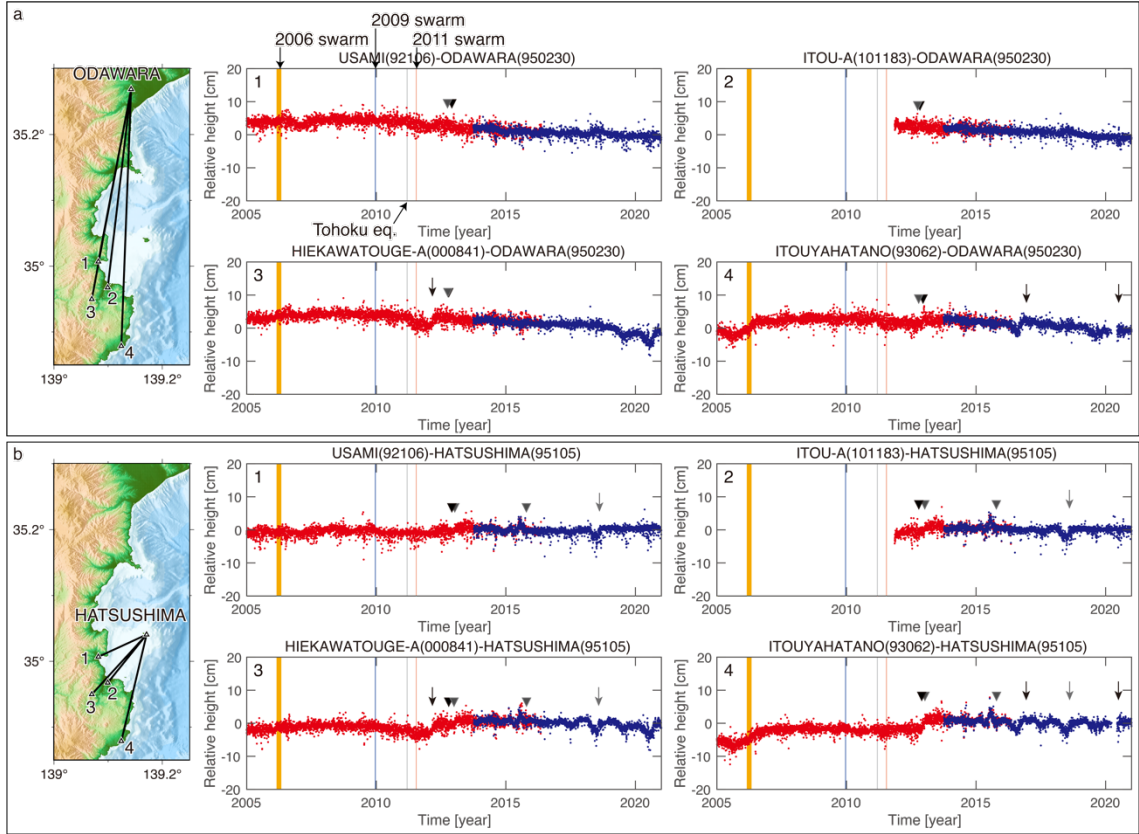


**Fig. 11.** Baseline changes. **a**, Left panel: Map showing stations (triangle) and baselines (segment). Reference station is ODAWARA, and stations 1, 2, 3, and 4 are USAMI, ITOU-A, HIEKAWATOUGE, and ITOUYAHATANO-A, respectively. Middle top panel: Relative heights of station 1 to the reference station as a function of time. Red and blue dots are F3 and F5 solutions, respectively. Orange, blue, and pink vertical lines indicate the moment of the 2006, 2009, and 2011 swarms, respectively. Right top panel: Same as the middle top panel for ITOU-A. Middle bottom panel: Same as the middle top panel for HIEKAWATOUGE. Right bottom panel: Same as the middle top panel for ITOUYAHATANO-A. Major maintenance: Triangle indicates antenna replacement of stations 1-4 (black) and the reference station (grey), and arrow indicates tree trimming around stations 1-4 (black) and the reference station (grey). **b**, Same as **a** for reference station HATSUSHIMA.

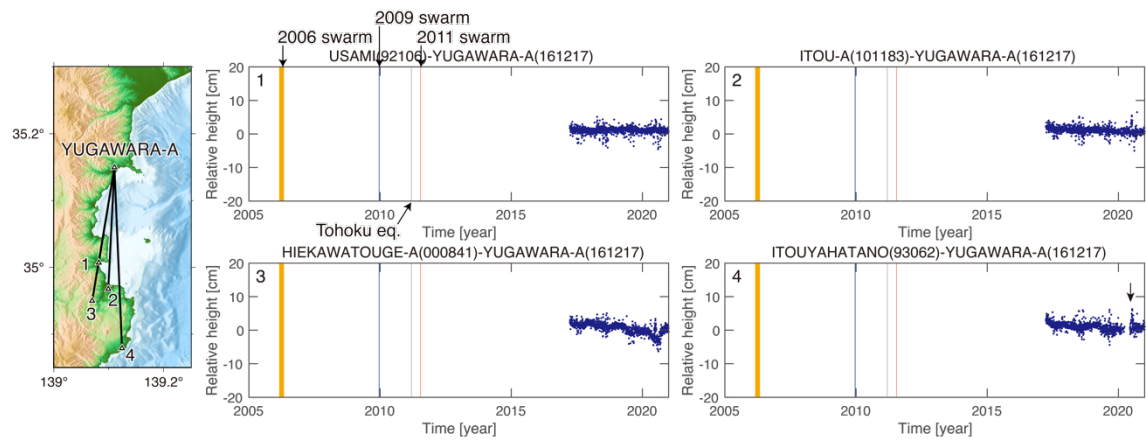


**Fig. 12.** Same as Fig. 11 for reference station YUGAWARA-A.